Thermodynamics of (Zn,Fe)S sphalerite. A CVM approach with large basis clusters

Article *in* Mineralogical Magazine · October 2000

DOI: 10.1180/002646100549751

2 authors, including:

Richard Sack
OFM Research
83 PUBLICATIONS **6,618** CITATIONS

SEE PROFILE

Mineralogical Magazine, October 2000, Vol. 64(5), pp. 923–943

Thermodynamics of (Zn,Fe)S sphalerite. A CVM approach with large basis clusters

A. I. BALABIN AND R. O. SACK*

Department of Geological Sciences, Box 351310, University of Washington, Seattle, WA 98195/1310, USA

ABSTRACT

We have developed a cluster variation method (CVM) model based on cuboctahedral and octahedral basis clusters containing 13 and 6 atoms, respectively, and applied it to the analysis of the thermodynamic mixing properties of (Zn,Fe)S solid solutions. The model, in which the internal energy of the lattice is approximated by next to nearest neighbour (*nnn*) pair interactions and many-body interactions associated with nearest neighbour (*nn*) equilateral triangles, describes the FeS contents of sphalerites equilibrated with pyrrhotite and pyrite, and with pyrrhotite and iron metal within experimental uncertainties. The model predicts moderate deviations from ideality; the mean values of the Lewis and Randall activity coefficient of FeS and ZnS are, 1.48 and 1.03, respectively. Predictions of the model are in qualitative agreement with cell-edge data. The model also predicts that sphalerites undergo long-range ordering to lower-symmetry structures at temperatures only slightly below those investigated experimentally, a result in agreement with inferences from an existing Mössbauer investigation of synthetic sphalerites.

More realistic models in which interactions are ascribed to larger species (*nn* triangular and centred square species) predict that such long-range ordering occurs at even higher temperatures and underscore the need for better characterization of the structures of (Zn,Fe)S minerals.

KEYWORDS: sphalerite, thermodynamics, cluster variation method, pyrrhotite, pyrite.

Introduction

THE Fe-bearing mineral solution sphalerite, (Zn,Fe)S, is a common constituent of polymetallic base-metal sulfide deposits and is also found in some iron meteorites. The phase equilibria, lattice dimensions, and activity-composition relations of sphalerites and phases with which it coexists have been investigated extensively to provide a basis for thermodynamic appraisal of the sphalerite solution adequate for quantifying the intensive parameters of ore-forming processes, metamorphism, and asteroid formation. Paradoxically, thermodynamic rationalization of the sphalerite solution has become progressively more controversial as increasing amounts of experimental data have become available. An ample retrospective account of this problem can be found in Toulmin *et al.* (1991) and references therein. The main problem at present is the difficulty in describing the data on FeS solubility in sphalerite coexisting in equilibrium with pyrrhotite and pyrite, within the framework of a simple solution model, and it is an even more challenging task to reconcile these measurements with data on more Fe-rich sphalerites equilibrated with pyrrhotite and metallic iron. Accordingly, we have undertaken a study to generate a more realistic solution model not suffering from this inadequacy.

In this paper we review the systematics of sphalerite relevant to constructing such a model. We then briefly discuss cluster variation method (CVM) models and outline the features of a CVM model with large basis clusters (cuboctahedron + octahedron) which we have developed and adapted for description of the thermodynamic properties of the sphalerite solution. Explicit expressions for the entropy, internal energy and

* E-mail: chukchi@u.washington.edu

volume for the cuboctahedron + octahedron CVM approximation are developed therein. We then discuss calibrations of our CVM models which successfully describe the extant experimental data. Finally, we summarize our results and briefly discuss some issues that need to be resolved before attempting applications to natural assemblages.

Systematics

The topology of the Zn-Fe-S phase diagram over the temperature range 325–742°C is identical to that given in Fig. 1 for 600°C. In this system sphalerite (Zn,Fe)S is a binary solid solution whose homogeneity range spans from 0 to ~56 mol.% FeS (at P = 1 bar and T = 450–900°). The compositions of the other phases of interest here, pyrite, pyrrhotite and Fe metal, in effect belong to the binary subsystem Fe-S. The sphalerite with maximum FeS content corresponds to its equilibrium with Fe metal and pyrrhotite, which in turn is nearly stoichiometric FeS. Pyrrhotites with higher sulfur contents (i.e. those with increasing deviation from stoichiometry) coexist with sphalerites whose FeS content diminishes progressively until the sulfur content of pyrrhotite reaches its maximum and pyrite joins the assemblage.

As first reported by Boorman (1967), the FeS solubility of sphalerite coexisting with pyrite and pyrrhotite is ~21 mol.% FeS at 1 bar, 550°C and

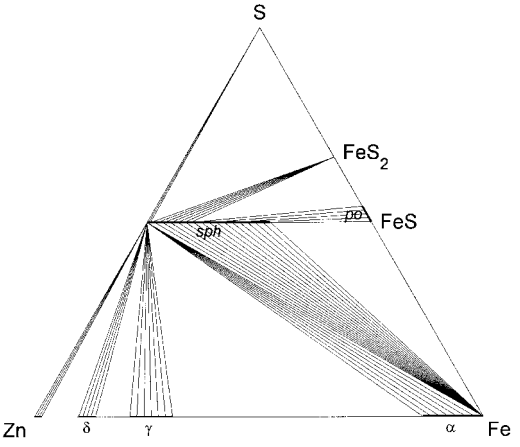

FIG. 1. Phase diagram of the Zn-Fe-S system at 600°C and 1 bar, based on data from Balabin and Urusov (1995), Barton and Toulmin (1966), and Massalski (1986).

remains virtually constant below this temperature. Subsequent studies (Scott and Barnes, 1971; Boorman *et al.*, 1971; Scott, 1973; Lusk and Ford, 1978) confirmed that the temperature effect on FeS solubility in sphalerite is negligible and indicated that the temperature below which the derivative

$$\frac{\partial N^{sp}_{FeS}}{\partial T} = 0$$

for this assemblage increases with increasing pressure (Fig. 1 in Lusk and Ford, or Fig. 5 in this paper). The composition of sphalerite in equilibrium with stoichiometric pyrrhotite and metallic Fe has also been well characterized experimentally at 1 bar (Barton and Toulmin, 1966; Balabin and Urusov, 1995) and at 2.5 and 5.0 kbar (Hutchison and Scott, 1983). At 1 bar the equilibrium solubility of FeS in sphalerite can be described with the equation

$$N^{Sph}_{FeS}\ (\text{mol.\%}) = 44.09 + 0.0125 \times T(\text{K}) \qquad (1)$$

with a standard error of $< \pm 0.5$ mol.% FeS (Balabin and Urusov, 1995).

Appraisals of the thermodynamic mixing properties of the sphalerite solution based on these data and those for higher variance assemblage sphalerite + pyrrhotite have proved problematic. It has been established that sphalerites with >22 mol.% FeS exhibit, at most, only moderate deviations from ideality (Barton and Toulmin, 1966; Fleet, 1975; Balabin and Urusov, 1995). Within the context of a simple solution model for sphalerite, this inference can not be reconciled with the data on the assemblage sphalerite + pyrrhotite + pyrite, because one needs to ascribe a very strong and peculiar variation to the compositional derivative of the activity coefficient

$$\left(\frac{\partial \ln \gamma^{sp}_{FeS}}{\partial N^{sp}_{FeS}}\right)_{P;T}$$

in order to account for the apparent verticality of the isobars of FeS solubility in sphalerite (Toulmin *et al.*, 1991). At the same time, the linear dependence of heat capacity of Fe-sphalerite on composition (Pankratz and King, 1965) implies negligible excess entropy of mixing in this solution. These issues need to be resolved before a model adequate for describing the thermodynamic properties of the low-FeS sphalerites characteristic of polymetallic base-metal sulfide deposits can be developed.

It is important to note that metastable phenomena may complicate experimental investigation of sphalerite below 500°C. For example,

there appears to exist another (metastable?) version of the equilibrium of sphalerite with pyrite and pyrrhotite in which the FeS content of sphalerite increases sub-linearly with decreasing temperature. These results, obtained by Chernyshev *et al.* (1968) and later confirmed by Sorokin and Chichagov (1974), have been largely dismissed by the community because the sphalerites in Chernyshev *et al.* (1968) exhibit sharp stepwise changes in the FeS content (Boorman *et al.*, 1971). However, similar inhomogeneities were later reported by Scott and Barnes (1971) and by Lusk and Ford (1978) in their run products. It appears that metastable phenomena may also explain similar inconsistencies among the data on FeS distribution between sphalerite and non-stoichiometric hexagonal pyrrhotite (Barton and Toulmin, 1966; Chernyshev *et al.*, 1968, 1969; Scott and Barnes, 1971; Sorokin and Chichagov, 1974; Sorokin and Bezmen, 1973; Bryndzia *et al.*, 1988); however, the higher variance of the latter assemblage makes this inference less certain.

Interpretation of lattice spacing for the Fe-sphalerite solution is also problematic. Barton and Toulmin (1966) established that the lattice parameter a_o of Fe-sphalerites synthesized under extremely low sulfur pressures controlled by the Fe/FeS buffer (dry sintering) depends on thermal history. Sphalerites synthesized by these authors at higher sulfur pressures did not show such variation, but corresponding values of a_o, when plotted against composition, were distributed with unusually wide dispersion around the fitting curve given by the expression:

$$a_o = 5.4093 + 0.0005637 N_{FeS}^{Sph} - 0.0004107 (N_{FeS}^{Sph})^2 \qquad (2)$$

where N_{FeS}^{Sph} is the mol.% of FeS in sphalerite. Below ~30 mol.% FeS the low-sulfur pressure points fit this curve very well, but at higher FeS contents they fall progressively further below the curve, the higher temperature runs departing from the curve more than the lower ones (Figs 2 and 3 in Barton and Toulmin, 1966; Fig. 6*a,b* in the present paper). Similarly, most of the data provided by other authors (van Aswegen and Verleger, 1960; Sorokin *et al.*,1970; Chernyshev *et al.*, 1969; Osadchii and Sorokin, 1989, Dicarlo *et al.*, 1990) are in good agreement with equation 19 below 20–25 mol.% FeS but deviate from it at higher FeS contents. The apparent spread of data points seems to widen for sphalerites synthesized hydrothermally at lower temperatures (Fig. 1 in Sorokin *et al.*, 1970; Fig. 1 in Chernyshev *et al.*, 1969).

The pyrrhotite solid solution which coexists with sphalerite, $Fe_{1-\delta}S$, possesses a wide field of stability. The Fe-rich limit of pyrrhotite is widely regarded as the essentially stoichiometric composition FeS, although there is indirect evidence that the pyrrhotite coexisting with α- or γ-iron is slightly Fe deficient (~$Fe_{0.993}S$, Keller-Besrest and Collin, 1990). On the sulfur-rich side, the limit of the pyrrhotite field is defined by saturation with pyrite, and this equilibrium has been extensively investigated (e.g. Arnold, 1962; Toulmin and Barton, 1964; Schneeberg, 1973; Udodov and Kashayev,1970; Chernyshev *et al.*, 1968; Scott, 1973). In all of these studies the composition of pyrrhotite was determined by the X-ray diffraction (XRD) method of Arnold (1962) as modified by Toulmin and Barton (1964). Subsequently, Fleet (1968) noted a discontinuity in the variation of lattice parameters and d_{102} of pyrrhotite at 48.8 atom.% Fe, a discontinuity that might indicate that the Fe contents of the above-mentioned pyrrhotites have been overestimated by up to 0.18 atom.%.

Numerous XRD, magnetic and Mössbauer spectroscopy studies have demonstrated that deficiencies in Fe are accommodated by vacancies on Fe sites in pyrrhotite (cf. Novikov *et al*, 1988). Libowitz (1972) showed that experimental measurements of sulfur activity in pyrrhotite at various temperatures and compositions (e.g. Rosenqvist, 1954; Toulmin and Barton, 1964; Niwa and Wada, 1961; Burgman *et al.*, 1968; Turkdogan, 1968; Rau, 1976) could be described assuming coexistence of two types of point defects: interacting Fe vacancies as the prevailing defect and interstitial Fe atoms as a complementary defect. More recently a Libowitz-type model of pyrrhotite was recalibrated by Chuang *et al.* (1985). It provides an accurate description of the activity of sulfur in sulfur-rich pyrrhotites, where complementary defects can be neglected. For nearly stoichiometric pyrrhotite, the sulfur activity becomes very sensitive to small changes in composition due to formation of complementary defects, with the consequence, that the chemical potential of FeS evaluated for the coexistence of pyrrhotite and Fe metal using the model of Chuang *et al.* (1985) may be imprecise.

Unfortunately, the volumetric data for high-temperature hexagonal pyrrhotite are sparse, although numerous measurements of volumes

for low-temperature (<320°C) polymorphs have been reported. In this study we adopt the equation of state for stoichiometric FeS derived by Balabin and Urusov (1995) from the experimental data of Taylor (1969), King and Prewitt (1982), Novikov *et al.* (1982), Anzai and Ozawa (1974). For nonstoichiometric pyrrhotite, $Fe_{1-\delta}S$, the following linear equation for the molar volume at room temperature

$$V_{Fe_{1-\delta}S}\ cm^3 = 18.366 - 6.231\delta,$$

may be obtained from least-squares fitting of the data from Fleet (1968), Novikov *et al.* (1982) and Kruse (1990), utilizing only points with $0.01258 \leqslant \delta \leqslant 0.05$ as representative of the NiAs structure with disordered, 'free' vacancies (Novikov *et al.*, 1988; Kruse, 1990). In the absence of any information on the thermal expansion and compressibility, we have assumed them to be the same as those of stoichiometric FeS. Finally, the molar volume of pyrite may be obtained from the room-conditions value 23.943 $cm^3 mol.^{-1}$ (Toulmin *et al.*, 1991) and thermal expansion and bulk modulus provided by Skinner (1962) and Benbattouche *et al.* (1989), respectively.

CVM models

The cluster variation method (CVM) encompasses a class of approximations for statistical mechanics of order-disorder in crystals originally suggested by Kikuchi (1951) and subsequently reformulated and extended by Barker (1953), Hijmans and de Boer (1955), and many others. An exhaustive historic account of CVM can be found in de Fontaine (1994). A characteristic of this method is the expression for the configurational entropy of a mixed crystal in terms of configurational probabilities of distinct atomic groups (clusters). Though this heuristic method has not received a rigorous mathematical proof, its efficacy was ascertained via calculations of critical temperatures, by *ab initio* calculations of alloy phase diagrams and comparison with those determined experimentally (de Fontaine, 1994), and more recently by Monte Carlo simulations (Finel, 1994).

A CVM approximation is usually established by assigning one or two groups of lattice sites to be the largest or basis clusters. Overlapping of adjacent clusters gives rise to a succession of smaller clusters called overlap figures, the smallest cluster being the lattice site itself. In a binary system, vertices of a cluster with r sites can be occupied by atoms of two kinds, say A and B, thereby generating 2^r distinctive configurations. These cluster configurations, however, are not independent. Application of CVM to a particular lattice pivots on enumeration of cluster configurations and description of their respective probabilities in terms of a relatively small number of independent variables.

Recent advances in CVM were accomplished using the so-called configurational polynomials as independent variables, an elegant algebraic technique suggested by Sanchez *et al.* (1984). This method made computations for clusters of up to 13 or 14 atoms feasible on supercomputers (de Fontaine, 1994). However, these calculations are too expensive to allow for data fitting, due to the iterative nature of this procedure. To make the practical applications feasible, a variety of simplified approaches to CVM have been proposed (Schlijper and Westerhof, 1987; Vinograd and Putnis, 1999; Oates *et al.*, 1999; Vaks and Samolyuk, 1999; among others), sacrificing some of the method's accuracy for computational tractability. Despite the importance of all these efforts, applications of CVM to the analysis of experimental data on phase equilibrium have been restricted to formalisms with basis clusters containing at most four to six atoms.

The wide use of correlational polynomials has overshadowed previous CVM approximations based on explicit formulation of the linear equations relating different cluster configurations, because the intricacy of these constraints renders such approximations extremely cumbersome to formulate for large clusters. Even so, CVM approximations based on the explicit formulation of the relevant linear equations have the advantage that they make the task of minimizing the Gibbs energy for equilibrium cluster probabilities much easier, as they can be accomplished with a simple and fast iteration technique proposed by Kikuchi (1973). In the present paper, an attempt is made to regain the computational ease of the earlier versions of CVM at the modern level of large basis clusters without ever using configurational polynomials. Our approach develops the principles formulated by Hijmans and de Boer (1955) and supplements them with special computer programs designed to itemize various cluster configurations and their mutual relations. A complete description of this modification of CVM with taxonomy of cluster configurations and derivations of linear constraints between them will be published

elsewhere. Only the essentials necessary for understanding our approach to the sphalerite solution are elaborated below.

Cuboctahedron + octahedron CVM approximation

In this paper we present a new CVM approximation for the *fcc* lattice, which is the cationic sublattice of sphalerite, with the thirteen-point cuboctahedron and six-point octahedron basis clusters. The choice of basis clusters, somewhat smaller that those in the best available 13+14 *fcc* treatment (de Fontaine, 1994), was motivated solely by potential numerical difficulties. No such difficulties were encountered in the course of our work, however, and we speculate that our approach may be extended to the 13+14 treatment and even larger clusters.

For the sake of convenience each cluster of interest will be designated with a bold italic symbol. The two basis clusters involved in the approximation are the cuboctahedron ***co*** [1,2,3,4,5,6,7,8,9,10,11,12,13] and the octahedron ***oh*** [11,13,6,7,14,2] shown in Fig. 2. The relevant overlap figures are (1) the double tetrahedron ***dt*** [1,5,4,2,6,13] arising from the overlap of two cuboctahedra; (2) the quadrilateral pyramid ***py*** [6,2,7,11,13] from the overlap of a cuboctahedron and an octahedron; (3) the regular tetrahedron ***th*** [1,4,5,13] from the overlap of two double-tetrahedra; (4) the irregular tetrahedron ***itd*** [1,13,5,6] from the overlap of an octahedron and a double-tetrahedron; (5) the square ***sq*** [1,2,3,4] from the overlap of two pyramids; (6) the equilateral triangle ***tr*** [1,2,3] from the overlap of an octahedron and a tetrahedron; (7) the right angular triangle ***rtr*** [1,3,13] shared by two irregular tetrahedra, (8) the first *nn* pair ***nn*** [1,2] given by the overlap of two adjacent tetrahedra, (9) the second *nn* pair ***nnn*** [6,7] from the overlap of two irregular tetrahedra; and the point 'cluster' ***po***. One more cluster of interest is the centred square ***csq*** [5,6,7,8,13]. This cluster, instrumental in the description of the internal energy, is an example of a subcluster (of ***co***) which is not an overlap figure (i.e. it cannot be obtained by overlap of adjacent basis clusters).

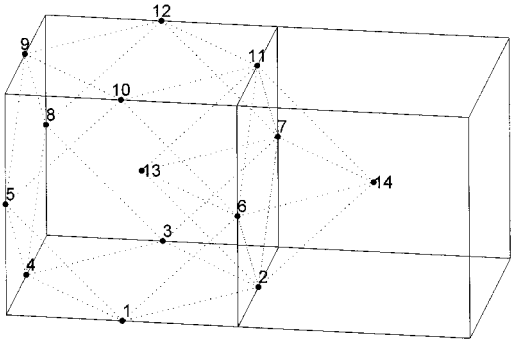

FIG. 2. Basis clusters used in the cuboctahedron-octahedron approximation.

In counting configurations, the probability of finding a cluster in a particular configuration should not depend on its orientation in the lattice where long-range ordering is absent. Correspondingly, the arrangements of atoms over vertices (nodes) of a cluster that can be obtained from each other by rotation or reflection in space are considered equivalent representatives of the same cluster configuration. The number of distinguishable atomic arrangements representative of a cluster configuration is characterized by a multiplicity number. To give a few specific examples needed later in this section for descriptions of configurational volume and internal energy, cluster configurations of ***tr***, ***csq*** and ***oh*** are shown Tables 1, 2 and 3, respectively.

For each cluster, an inventory of all different configurations can be generated with special computer programs. There are 288 different configurations of ***co***, 10 of ***oh***, 21 of ***dt***, 12 of ***py***, 5 of ***td***, 6 of ***sq***, 9 of ***itd***, 4 of ***tr***, 3 of ***nn***, 3 of ***nnn***, 2 of ***po*** and 12 of ***csq***. The multiplicity of these configurations can be calculated using the so-called Orbit-Stabilizer theorem, a result from group theory (Cromwell, 1997, p. 408). The numerical order in which the configurations of a cluster ***a*** are put in its inventory may be arbitrary, but once set down it should be kept the same throughout for consistency. Therefore each configuration of ***a*** is assigned an ordinal

TABLE 1. Cluster-configurations of Triangular [1,2,3].

o.n.	Configuration	Multiplicity
1	AAA	1
2	AAB	3
3	ABB	3
4	BBB	1

TABLE 2. Cluster-configurations of centred square [5,6,7,8,13].

o.n.	Configuration	Multiplicity
1	AAAAA	1
2	BAAAA	4
3	BBAAA	4
4	BABAA	2
5	BBBAA	4
6	BBBBA	1
7	AAAAB	1
8	BAAAB	4
9	BBAAB	4
10	BABAB	2
11	BBBAB	4
12	BBBBB	1

number. The symbol α_i^a will be used to denote the multiplicity of the i'th configuration of the cluster $\boldsymbol{a}$. For instance $\alpha_1^{tr} = 1$; $\alpha_2^{tr} = 3$; $\alpha_4^{oh} = 3$, etc. (Tables 1 and 3). Generally, the ith configuration of the cluster $\boldsymbol{a}$ can be realized by α_i^a distinguishable atomic arrangements, each of which has the same probability. This probability (i.e. the probability of one particular arrangement representative of the ith configuration of $\boldsymbol{a}$) will be denoted p_i^a; accordingly, the probability of finding the cluster $\boldsymbol{a}$ in its ith configuration equals $\alpha_i^a p_i^a$. It is convenient to arrange the probabilities p_i^a as components of a column vector $\mathbf{p}^a$

$$\mathbf{p}^a = \begin{bmatrix} p_1^a \\ p_2^a \\ \cdots \\ \cdots \\ p_m^a \end{bmatrix}$$

here, following conventional notation, the vector is designated by a bold symbol and its components by italic ones.

For any two clusters $\boldsymbol{a}$ and $\boldsymbol{b}$ the symbol $M(\boldsymbol{a},\boldsymbol{b})$ will be used to indicate the number of figures of type $\boldsymbol{b}$ contained in a figure of type $\boldsymbol{a}$ (by

TABLE 3. Cluster-configurations of octahedron [11,13,6,7,14,2].

o.n.	Configuration	Multiplicity	Volume†
1	AAAAAA	1	$\frac{\sqrt{2}}{3} d_{\mathrm{A-A}}^3$
2	BAAAAA	6	$\frac{d_{\mathrm{A-A}}^2}{3}\left(\sqrt{d_{\mathrm{A-B}}^2 - \frac{d_{\mathrm{A-A}}^2}{2}} + \frac{d_{\mathrm{A-A}}}{\sqrt{2}}\right)$
3	ABBAAA	12	$\frac{d_{\mathrm{A-A}}}{6}(d_{\mathrm{A-A}} + d_{\mathrm{B-B}})\sqrt{3d_{\mathrm{A-B}}^2 - d_{\mathrm{A-A}}^2 + d_{\mathrm{A-A}} d_{\mathrm{B-B}} - d_{\mathrm{B-B}}^2}$
4	ABAABA	3	$\frac{d_{\mathrm{A-A}}^2}{3}\sqrt{4d_{\mathrm{A-B}}^2 - 2d_{\mathrm{A-A}}^2}$
5	BBBAAA	8	$\frac{1}{12}(d_{\mathrm{A-A}} + d_{\mathrm{B-B}})^2\sqrt{3d_{\mathrm{A-B}}^2 - d_{\mathrm{A-A}}^2 + d_{\mathrm{A-A}} d_{\mathrm{B-B}} - d_{\mathrm{B-B}}^2}$
6	ABBABA	12	$\frac{1}{6}\left(d_{\mathrm{A-A}}^2\sqrt{4d_{\mathrm{A-B}}^2 - 2d_{\mathrm{A-A}}^2} + d_{\mathrm{B-B}}^2\sqrt{4d_{\mathrm{A-B}}^2 - 2d_{\mathrm{B-B}}^2}\right)$
7	AABBBB	12	$\frac{d_{\mathrm{B-B}}^2}{6}(d_{\mathrm{A-A}} + d_{\mathrm{B-B}})\sqrt{3d_{\mathrm{A-B}}^2 - d_{\mathrm{A-A}}^2 + d_{\mathrm{A-A}} d_{\mathrm{B-B}} - d_{\mathrm{B-B}}^2}$
8	ABBBBA	3	$\frac{d_{\mathrm{B-B}}^2}{3}\sqrt{4d_{\mathrm{A-B}}^2 - 2d_{\mathrm{B-B}}^2}$
9	ABBBBB	6	$\frac{d_{\mathrm{B-B}}^2}{3}\left(\sqrt{d_{\mathrm{A-B}}^2 - \frac{d_{\mathrm{B-B}}^2}{2}} + \frac{d_{\mathrm{B-B}}}{\sqrt{2}}\right)$
10	BBBBBB	1	$\frac{\sqrt{2}}{3} d_{\mathrm{B-B}}^3$

† The formulae for the volume of the octahedron in its different configurations were provided by Prof. Idj. Kh. Sabitov and his associates at Moscow State University.

convention $M(\boldsymbol{a},\boldsymbol{b}) = 0$ if $\boldsymbol{b}$ is not a subcluster of $\boldsymbol{a}$). The total number of figures of type $\boldsymbol{a}$ in the lattice containing N sites will be indicated by $\chi^a N$. The coefficients $M(\boldsymbol{a},\boldsymbol{b})$ and χ^a for all clusters relevant to our CVM formalism for the *fcc* lattice are assembled in Table 4.

Every pair of clusters $\boldsymbol{a}$ and $\boldsymbol{b}$ such that $\boldsymbol{b}$ is a subcluster of $\boldsymbol{a}$ will have associated with them a matrix Γ^a_b in which the (i,j) entries are the numbers of jth configurations of $\boldsymbol{b}$ contained in the ith configuration of $\boldsymbol{a}$. Matrices of this type play a central role in our calculations; the computer code written for generating them will be described elsewhere.

If the configurational probabilities of a cluster $\boldsymbol{a}$ are known, the corresponding probabilities for its subclusters $\boldsymbol{b}$ can be calculated according to the formula

$$\mathbf{p}^b = \frac{1}{M(a;b)} diag^{-1}\{\alpha_1^b,\alpha_2^b,\ldots\ \alpha_n^b\}\ \Gamma^a_b\ diag\{\alpha_1^a,\alpha_2^a,\ldots\alpha_m^a\}\mathbf{p}^a \qquad (3)$$

where $diag\{\ldots\}$ and $diag^{-1}\{\ldots\}$ denote a diagonal matrix and its inverse. Using this formula the configurational probabilities for all clusters in the approximation can be expressed as linear forms in the probabilities of the largest (i.e. basis) clusters. As $\boldsymbol{co}$ and $\boldsymbol{oh}$ are the basis clusters in the CVM approximation under consideration, the probabilities of all other clusters are linear functions of 288 components of $\mathbf{p}^{co}$ and 10 components of $\mathbf{p}^{oh}$. However, the configurational probabilities of the basis clusters are not independent: First, they must satisfy the normalizing conditions

$$\sum_{i=1}^{288}\alpha_i^{co}p_i^{co} = 1 \quad \text{and} \quad \sum_{i=1}^{10}\alpha_i^{oh}p_i^{oh} = 1 \qquad (4)$$

Next, the probabilities of cluster configurations must satisfy consistency conditions imposed by the topology of the crystal lattice (i.e. the way in which the clusters are pieced together to constitute the lattice). The nature of these constraints can be illustrated, for example, by considering all clusters containing $\boldsymbol{itd}$ as a subcluster, namely $\boldsymbol{py}$, $\boldsymbol{oh}$, $\boldsymbol{dt}$ and $\boldsymbol{co}$ (cf. Table 4). We can use equation 3 to express the vector $\mathbf{p}^{itd}$ in terms of the vectors $\mathbf{p}^{py}$, $\mathbf{p}^{oh}$, $\mathbf{p}^{dt}$ or $\mathbf{p}^{co}$, but the configurational probabilities for $\boldsymbol{itd}$ in the lattice do not depend on the way of calculations, requiring that the components of $\mathbf{p}^{py}$, $\mathbf{p}^{oh}$, $\mathbf{p}^{dt}$ and $\mathbf{p}^{co}$ satisfy the following systems of linear equations:

$$\frac{1}{M(\text{py;itd})}\Gamma^{py}_{itd}diag\{\alpha_1^{py},\alpha_2^{py},\ldots\alpha_{12}^{py}\}\mathbf{p}^{py} = \frac{1}{M(\text{oh;itd})}\Gamma^{oh}_{itd}diag\{\ \alpha_1^{oh},\alpha_2^{oh},\ldots\alpha_{10}^{oh}\}\mathbf{p}^{oh}$$

$$\frac{1}{M(\text{oh;itd})}\Gamma^{oh}_{itd}diag\{\ \alpha_1^{oh},\alpha_2^{oh},\ldots\alpha_{10}^{oh}\}\mathbf{p}^{oh} = \frac{1}{M(\text{dt;itd})}\Gamma^{dt}_{itd}diag\{\ \alpha_1^{dt},\alpha_2^{dt},\ldots\alpha_{21}^{dt}\}\mathbf{p}^{dt}$$

$$\frac{1}{M(\text{dt;itd})}\Gamma^{dt}_{itd}diag\{\ \alpha_1^{dt},\alpha_2^{dt},\ldots\alpha_{21}^{oh}\}\mathbf{p}^{dt} = \frac{1}{M(\text{co;itd})}\Gamma^{co}_{itd}diag\{\ \alpha_1^{co},\alpha_2^{co},\ldots\alpha_{288}^{co}\}\mathbf{p}^{co}$$

for each of the terms above equals $diag\{\alpha_1^{itd},\alpha_2^{itd},\ldots\alpha_{288}^{itd}\}\mathbf{p}^{itd}$. Using equation 3 repeatedly and substituting the corresponding numbers from Table 1 for $M(\boldsymbol{py},\boldsymbol{itd})$, $M(\boldsymbol{oh},\boldsymbol{py})$, $M(\boldsymbol{oh},\boldsymbol{itd})$, $M(\boldsymbol{dt},\boldsymbol{itd})$ and $M(\boldsymbol{co},\boldsymbol{dt})$, $M(\boldsymbol{co},\boldsymbol{itd})$, these equations may be restated as constraints on the configurational probabilities of the basis clusters $\mathbf{p}^{oh}$ and $\mathbf{p}^{co}$:

TABLE 4. Entropy coefficients $M(\boldsymbol{b},\boldsymbol{a})$, $\gamma(\boldsymbol{a})$, and χ^a for cuboctahedron + octahedron approximations.

	po	***nn***	***nnn***	***rtr***	***tr***	***itd***	***sq***	***td***	***csq***	***py***	***dt***	***oh***	***co***	γ	χ
po	1	2	2	3	3	4	4	4	5	5	6	6	13	1	0
nn	0	1	0	2	3	5	4	6	4	8	11	12	36	6	0
nnn	0	0	1	1	0	1	2	0	4	2	2	3	12	3	0
rtr	0	0	0	1	0	2	4	0	4	4	4	12	36	12	0
tr	0	0	0	0	1	2	0	4	0	4	8	8	32	8	−8
itd	0	0	0	0	0	1	0	0	0	4	2	12	24	12	12
sq	0	0	0	0	0	0	1	0	0	1	0	3	6	3	0
td	0	0	0	0	0	0	0	1	0	0	2	0	8	2	6
csq	0	0	0	0	0	0	0	0	1	0	0	0	6	3	0
py	0	0	0	0	0	0	0	0	0	1	0	6	6	6	−6
dt	0	0	0	0	0	0	0	0	0	0	1	0	12	6	−6
oh	0	0	0	0	0	0	0	0	0	0	0	1	0	1	1
co	0	0	0	0	0	0	0	0	0	0	0	0	1	1	1

$$\left(\tfrac{1}{4}\Gamma^{py}_{itd} diag\left\{\alpha^{py}_1;\alpha^{py}_2;:::\alpha^{py}_{12}\right\}\tfrac{1}{6}\Gamma^{oh}_{py} - \tfrac{1}{12}\Gamma^{oh}_{itd}\right) diag\{\alpha^{oh}_1,\alpha^{oh}_2,...\alpha^{oh}_{10}\}\mathbf{p}^{oh} = 0$$

$$\tfrac{1}{12}\Gamma^{oh}_{itd} diag\left\{\alpha^{oh}_1;\alpha^{oh}_2;:::\alpha^{oh}_{10}\right\}\mathbf{p}^{oh} = \tfrac{1}{2}\Gamma^{dt}_{itd} diag\left\{\alpha^{dt}_1;\alpha^{dt}_2;:::\alpha^{dt}_{21}\right\}\tfrac{1}{12}\Gamma^{co}_{dt} diag\left\{\alpha^{co}_1;\alpha^{co}_2;:::\alpha^{co}_{288}\right\}\mathbf{p}^{co}$$

$$\tfrac{1}{2}\left(\Gamma^{dt}_{itd} diag\left\{\alpha^{dt}_1;\alpha^{dt}_2;:::\alpha^{dt}_{21}\right\}\tfrac{1}{12}\Gamma^{co}_{dt} - \tfrac{1}{24} diag\Gamma^{co}_{itd}\right) diag\left\{\alpha^{co}_1;\alpha^{co}_2;:::\alpha^{co}_{288}\right\}\mathbf{p}^{co} = 0$$

Similar equations involving configurational probabilities of all the pairs of clusters sharing a common subcluster can be readily established, notwithstanding the fact that the bulk of them may be redundant. The complete set of constraints obtained in this way for the current cuboctahedron + octahedron approximation amounted to 153 linear equations. However, the whole system was found to be of rank thirteen, signifying that any thirteen linearly independent equations of the whole set will suffice to represent the complete set of the desired consistency constraints, the remaining equations being their linear combinations. The coefficients of these thirteen linearly independent constraints were assembled as a 13 by 298 matrix **A**, the constraints themselves being of the form

$$\mathbf{A}\begin{bmatrix}\mathbf{p}^{co}\\ \mathbf{p}^{oh}\end{bmatrix} = 0 \qquad (5)$$

Yet another group of constraints is imposed by the general thermodynamic principle that the Gibbs energy G

$$G = U + PV - TS \qquad (6)$$

where U stands for the internal energy, V for the volume, and S for the entropy, attains its minimum at the equilibrium configuration of the lattice provided the temperature T pressure P and masses of the two components in the solution are kept constant. The condition that masses of the components be kept constant can be expressed either as

$$\Gamma^{oh}_{po} diag\left\{\alpha^{oh}_1;\alpha^{oh}_2;:::\alpha^{oh}_{10}\right\}\mathbf{p}^{oh} = \begin{bmatrix}1-x\\ x\end{bmatrix} \qquad (7)$$

or

$$\Gamma^{co}_{po} diag\left\{\alpha^{co}_1;\alpha^{co}_2;:::\alpha^{co}_{288}\right\}\mathbf{p}^{co} = \begin{bmatrix}1-x\\ x\end{bmatrix} \qquad (8)$$

where x is the mole fraction of the second component; note that Γ^{oh}_{po} and Γ^{co}_{po} are 2 by 288 and 2 by 10 matrices, respectively.

By virtue of the consistency conditions (equation 5), the terms in the left hand sides of the last two systems of equations are equal to each other. Therefore it will suffice to fulfill either of the equations 7 or 8 to qualify for fulfillment of the other. Furthermore, it can be shown that whenever the pair of systems 5 and 7 or 5 and 8 are satisfied, the normalizing conditions (equations 4) are satisfied also. Hence systems 5 and 7 will represent the complete set of constraints.

Finally, being positive by nature, the cluster probabilities should satisfy the inequalities

$$\mathbf{p}^{co}_i > 0,\ i = 1,2,...298;\ \text{and}\ \mathbf{p}^{oh}_j > 0,\ j = 1,2,...10 \qquad (9)$$

To summarize, given any temperature T, pressure P, and concentration x, the Gibbs energy G of the solution is to be minimized over a bounded convex polyhedron determined (in the 298-dimensional space spanned by the vectors $\mathbf{p}^{co}$ and $\mathbf{p}^{oh}$) by 15 linear constraints furnished by the systems 5 and 7 along with the inequalities 9. The independent components of G, the entropy S, the internal energy U and the volume V may be expressed explicitly as functions of the vectors $\mathbf{p}^{co}$ and $\mathbf{p}^{oh}$ as given below.

Entropy

The configurational entropy is described in CVM as a function of configurational probabilities of the basis clusters and their overlap figures by expression of the type

$$S^a = -Nk_B\sum_l \alpha^a_l p^a_l \ln p^a_l \qquad (10)$$

where k_B is the Boltzman constant, N is the total number of lattice points, and l runs over all of the configurations of the cluster $\boldsymbol{a}$, their respective probabilities p^a_l and multiplicity factors α^a_l being determined as above. The entropy is given as follows:

$$S = \sum_{a_i}\gamma(\boldsymbol{a}_i)S^{a_i} \qquad (11)$$

where the summation spans over all the basis clusters and overlap figures and where the entropy coefficients $\gamma(\boldsymbol{a}_i)$ are calculated recursively by the following rule: $\gamma(\boldsymbol{co}) = -\chi^{co} = -1$ and $\gamma(\boldsymbol{oh}) = -\chi^{oh} = -1$ for the basis clusters and $\gamma(\boldsymbol{a}) = -\chi^a - \sum_{a\subset b} M(\boldsymbol{b},\boldsymbol{a})\gamma(\boldsymbol{b})$ for any overlap-figure $\boldsymbol{a}$. In the latter formula the summation is performed over the basis clusters and all the overlap figures containing $\boldsymbol{a}$ as a subcluster. The entropy

coefficients obtained in this way are presented in the last column of Table 4. Substituting these coefficients into equation 11, we obtain the following formula for the entropy:

$$S = S^{co} + S^{oh} - 6S^{dt} + 6S^{td} - 6S^{py} + 12S^{itd} - 8S^{tr} \quad (12)$$

To estimate the entropy at a particular probability distribution represented by vectors and $\mathbf{p}^{co}$ and $\mathbf{p}^{oh}$, the configuration probabilities of the five overlap figures $\mathbf{p}^{dt}$, $\mathbf{p}^{td}$, $\mathbf{p}^{py}$, $\mathbf{p}^{itd}$ and $\mathbf{p}^{tr}$ need be calculated from them according to equation 3. Thereafter the entropy terms participating in equation 12 are calculated by equation 10.

Internal energy

The internal energy of the lattice is approximated as an additive function of the mole numbers of specific atomic groups, assuming that interactions in the lattice operate only within these (presumably small) molecular-type groups or 'species'. Thence the internal energy can be described by a linear form in the configuration probabilities of the basis clusters, provided care has been taken to select basis clusters large enough to include the energy-embodying species as subclusters. In principle, every configuration of each of the basis clusters possesses its own particular energy, and there are as many independent energy parameters as there are independent cluster probabilities (283 in this case). However, in the description of the experimental data, it is necessary to limit the number of adjustable variables to a minimum, the energy being expressed in terms of a few empirical interaction parameters accounting for prevailing interactions. For instance, if only pairwise interactions of neighbouring atoms are taken into account, the configurational energy of the lattice will be described with the familiar interchange energy

$$w^{nn} = \varepsilon_1^{nn} + \varepsilon_3^{nn} - 2\varepsilon_2^{nn} \quad (13)$$

where, ε_1^{nn}, ε_2^{nn} and ε_3^{nn} are the energies of A–A, A–B, and B–B ***nn*** bonds, respectively.

Where long-range interactions may not be neglected, larger species are invoked to create more fitting parameters until all the available data can be reproduced within experimental accuracy. Three methods of energy calculations were examined in the present study using the following 'species': (1) ***nn*** + ***nnn***, (2) ***tr*** + ***nnn***, and (3) ***tr*** + ***csq***. Since ***nn*** is a subcluster of ***tr***, the second method embraces the first as a special case. The second method is, in turn, inferior to the third inasmuch as ***nnn*** is a subcluster of ***csq***.

Similarly to the case of pairwise interactions, the configurational energy of the lattice is described with linear combinations of the energies of the selected 'species'. In the first case the energy is comprised of nearest neighbour and next to nearest neighbour interactions and is completely described with two parameters, the interchange energy w^{nn} given above and an analogous parameter w^{nnn} accounting for the energy of the ***nnn*** interactions,

$$w^{nnn} = \varepsilon_1^{nnn} + \varepsilon_3^{nnn} - 2\varepsilon_2^{nnn} \quad (14)$$

In equation 14 ε_1^{n}, ε_2^{nnn} and ε_3^{nnn} are the energies of A–A, A–B, and B–B ***nnn*** bonds, respectively. Thus the internal energy per lattice site is

$$E = (1 - x)E_A + xE_B - 6w^{nn}p_2^{nnn} - 3w^{nnn}p_2^{nnn} \quad (15)$$

where E_A and E_B are internal energies of the end-members.

Three parameters are needed to describe the interactions embodied by ***tr*** and ***nnn***: the w^{nnn} given by equation 14 and $w_1^{tr} = \varepsilon_1^{tr} - 3\varepsilon_3^{tr} + 2\varepsilon_4^{tr}$ and $w_2^{tr} = \varepsilon_2^{tr} - 2\varepsilon_3^{tr} + \varepsilon_4^{tr}$, where ε_i^{tr}, i = 1 to 4, are energies of the ***tr*** configurations, as shown in Table 1. In this case the internal energy per lattice site can be written as

$$E = (1 - x)E_A + xE_B - \tfrac{8}{3}w_1^{tr}(2p_2^{tr} + p_3^{tr}) + 8w_2^{tr}p_2^{tr} - \tfrac{3}{2}w^{nnn}p_2^{nnn} \quad (16)$$

Finally, the following ten parameters arise in the description of the energy in terms of ***tr*** and ***csq*** species:

$$w_1^{tr+csq} = \varepsilon_1^{tr} - 3\varepsilon_3^{tr} + 2\varepsilon_4^{tr} + 4\varepsilon_5^{csq} - 4\varepsilon_6^{csq} - 4\varepsilon_{11}^{csq} + 4\varepsilon_{12}^{csq}$$

$$w_2^{tr+csq} = \varepsilon_2^{tr} - 2\varepsilon_3^{tr} + \varepsilon_4^{tr} + \varepsilon_5^{csq} - \varepsilon_6^{csq} - \varepsilon_{11}^{csq} + \varepsilon_{12}^{csq}$$

$$w_3^{tr+csq} = \varepsilon_1^{csq} - 4\varepsilon_5^{csq} + 3\varepsilon_6^{csq}$$

$$w_4^{tr+csq} = \varepsilon_2^{csq} - 3\varepsilon_5^{csq} + 2\varepsilon_6^{csq}$$

$$w_5^{tr+csq} = \varepsilon_3^{csq} - 2\varepsilon_5^{csq} + \varepsilon_6^{csq}$$

$$w_6^{tr+csq} = \varepsilon_4^{csq} - 2\varepsilon_5^{csq} + \varepsilon_6^{csq}$$

$$w_7^{tr+csq} = \varepsilon_7^{csq} - 4\varepsilon_{11}^{csq} + 3\varepsilon_{12}^{csq}$$

$$w_8^{tr+csq} = \varepsilon_8^{csq} - 3\varepsilon_{11}^{csq} + 2\varepsilon_{12}^{csq}$$

$$w_9^{tr+csq} = \varepsilon_9^{csq} - 2\varepsilon_{11}^{csq} + \varepsilon_{12}^{csq}$$

$$w_{10}^{tr+csq} = \varepsilon_{10}^{csq} - 2\varepsilon_{11}^{csq} + \varepsilon_{12}^{csq}$$

Here ε_i^{csq}, i = 1 to 12, stand for the energies of configurations of ***csq*** as shown in Table 2. In this approach, the formula for the internal energy (see equation 17 below) may be readily derived, but, like equations 13–16, the derivation is too lengthy to reproduce here. It exploits the fact that the internal energy is represented by a linear form in variables $\boldsymbol{p}^{co}$ and $\boldsymbol{p}^{oh}$ (i.e. it may be thought of as a vector in the linear subspace conjugate to the linear manifold determined by the constraints given by equations 4 and 5).

Volume

The description of the configuration volume offers certain difficulties in CVM. Although a variety of approaches has been devised (e.g. Finel and Tetot, 1996; Zunger, 1994), none of them is instrumental in describing experimental data on the volume of a mixed crystal in terms of a small number of adjustable parameters. In this paper we present a new formalism henceforth called the 'bond-length approximation' that serves this purpose.

There are three kinds of bonds connecting nearest neighbouring atoms in the crystal, namely A–A, A–B and B–B. We assume that the length of each of these bonds is constant regardless of atomic configurations in the next to nearest and more distant milieu. As shown below, this assumption allows for the complete description of the volume for the *fcc* lattice in terms of three parameters.

Consider the system of all the planes (111) passing through nodes of the *fcc* lattice. (There are four such planes passing through every lattice site.) These planes cut the lattice into tetrahedra and octahedra. Inasmuch as these polyhedra (corresponding to the clusters ***th*** [1,4,5,13] and ***oh*** [11,13,6,6,14,2] of our CVM formalism, Fig. 2) cover the space without holes or duplication, their volumes add up to the volume of the entire lattice. Moreover, the volumes of both the tetrahedron and the octahedron can be calculated from the lengths of their edges. However these edges consist of ***nn*** bonds. Therefore, the lengths of the ***nn*** bonds (i.e. the distances A–A, A–B, and B–B) uniquely determine the volumes of ***th*** or ***oh*** in their respective configurations. Hence the problem of determining the configuration volume of the lattice reduces to calculation of the volumes of the tetrahedra and octahedra.

Let v_i^{oh} and v_j^{th} denote volumes of octahedron ***oh*** in its ith configuration and tetrahedron ***th*** in its jth configuration, respectively. In view of the above, the configurational volume V can be expanded as

$$V = N\sum_{i=1}^{10}\alpha_i^{oh}v_i^{oh}p_i^{oh} + 2N\sum_{j=1}^{5}\alpha_j^{th}v_j^{th}p_j^{th} \qquad (18)$$

Let $d_{\mathrm{A-A}}$, $d_{\mathrm{A-B}}$ and $d_{\mathrm{B-B}}$ denote the distances A–A, A–B and B–B, respectively. The explicit formula expressing the volume of the tetrahedron as a function of the edge lengths is well known (e.g. Bronshtein and Semendiaef, 1979, p. 187). Formulae for the volume of the octahedron in its various configurations are shown in Table 3. (The formulae for the volume of the octahedron in its different configurations were provided by Prof. Idj. Kh. Sabitov and his associates at Moscow State University.) Considering the distances between neighbouring atoms $d_{\mathrm{A-A}}$, $d_{\mathrm{A-B}}$ and $d_{\mathrm{B-B}}$ as adjustable empirical parameters, calculation of the configuration volumes $\boldsymbol{v}_i^{oh}$ and $\boldsymbol{v}_j^{th}$, upon substituting them into equation 18, yields the configurational volume of the mixed crystal at any given configurational probabilities $\mathbf{p}^{co}$ and $\mathbf{p}^{oh}$, the vector $\mathbf{p}^{th}$ being calculated from $\mathbf{p}^{co}$ by equation 3.

Gibbs energy minimization

Equations 6 and 18, and one of the equations 15, 16 or 17, and with all necessary substitutions, together describe the Gibbs free energy G as a function of P, T, vectors and $\mathbf{p}^{co}$ and $\mathbf{p}^{oh}$, selected energetic parameters and interatomic distances. The composition of the crystal is taken into account indirectly via equation 7.

The search for the equilibrium probability distribution of basis clusters that affords a

$$E = (1-x)E_{\mathrm{A}} + xE_{\mathrm{B}} - \tfrac{8}{3}w_1^{tr+csq}(2p_2^{tr} + p_3^{tr}) + 8w_2^{tr+csq}p_2^{tr} -$$
$$3w_3^{tr+csq}\left(\frac{13}{16}p_2^{csq} + \frac{5}{8}p_3^{csq} + \frac{5}{8}p_4^{csq} + \frac{7}{16}p_5^{csq} + \frac{1}{4}p_6^{csq} + \frac{3}{4}p_7^{csq} + \frac{9}{16}p_8^{csq} + \frac{3}{8}p_9^{csq} + \frac{3}{8}p_{10}^{csq} + \frac{3}{16}p_{11}^{csq}\right) +$$
$$3(w_4^{tr+csq}p_2^{csq} + w_5^{tr+csq}p_3^{csq} + w_6^{tr+csq}p_4^{csq} + w_7^{tr+csq}p_7^{csq} + w_8^{tr+csq}p_8^{csq} + w_9^{tr+csq}p_9^{csq} + w_{10}^{tr+csq}p_{10}^{csq}) \qquad (17)$$

minimum to the Gibbs energy G is the final task (and ultimate challenge) in development of a CVM formalism. Two numerical techniques have been elaborated for solving this problem during the present investigation. The first method utilizes the Newton-Raphson procedure. First, 283 of the 298 basis cluster probabilities (i.e. components of vectors $\mathbf{p}^{co}$ and $\mathbf{p}^{oh}$) are chosen as independent variables. The remaining fifteen basis cluster probabilities are expressed explicitly in terms of the independent ones through equations 5 and 7, and, in so doing, G is represented as a function of 283 variables. Explicit expressions for the first and second differentials of G with respect to the independent variables are obtained using the Chain Rule. The function G is then minimized with the standard Newton-Raphson iterative method (Saati and Bram, 1964, p. 56), which involves inversion of a 283 by 283 matrix of second partial derivatives at each iteration. A special recursive procedure that yields the exact inverse to the matrix of second differentials in a finite number of steps was devised to facilitate the computations both in speed and accuracy.

The second method implemented for minimization of the Gibbs free energy was similar to the so-called natural iteration technique suggested by Kikuchi (1973). This method represents a contraction point algorithm with essential use of Lagrange multipliers. A coherent description of these algorithms will be provided elsewhere. Using the random distribution as a starting point, the Newton-Raphson algorithm was found to converge in six to fifteen iterations, whereas the natural iteration method converges within 150–350 steps. However, the computations are less intricate in the latter so that both methods matched each other in terms of total computational time (1–3 s for calculations performed on computers employing the Pentium PRO microprocessor).

Optimization procedure

Calibration of a model for the sphalerite solution involves simultaneous optimization of the available thermodynamic and phase equilibrium data for the system Zn-Fe-S. In our thermodynamic appraisal of the sphalerite we have focused on the experimental results for the low-variance three-phase assemblages sphalerite + pyrrhotite + metallic Fe and sphalerite + pyrrhotite + pyrite. The data on distribution of FeS between sphalerite and pyrrhotite were not used in the present study in view of the increased difficulty in distinguishing stable from metastable runs for this higher-variance assemblage. Further, we have integrated the description of configurational volume furnished by the bond-length approximation into this appraisal.

First, let us consider the equilibrium of sphalerite with pyrrhotite and metallic Fe. In this assemblage the chemical potential of FeS in sphalerite is equal to the molar Gibbs energy of coexisting (stoichiometric) pyrrhotite. Even though the existing estimates of the latter quantity may be of somewhat dubious validity (see above), its pressure slope can be evaluated with sufficient accuracy from measurements of the molar volume, thermal expansion and compressibility of pyrrhotite. Correspondingly, the thermodynamic mixing properties of sphalerite can be evaluated using the following relation:

$$\mu^{Sph}_{FeS}(P,T,x_1) - \mu^{Sph}_{FeS}(1\ \text{bar}, T, x_0) = \int_{1\text{bar}}^{P} V_{FeS}\,dP = \varphi(T,P) \qquad (19)$$

where x_0 denotes the solubility of FeS in sphalerite saturated with stoichiometric pyrrhotite at some temperature T when the pressure equals 1 bar; x_1 stands for the solubility of FeS in sphalerite at the same temperature T when pressure is increased to P. V_{FeS} is the standard molar volume of stoichiometric pyrrhotite and the explicit expression of $\varphi(T,P) = \int_{1\text{bar}}^{P} V_{FeS}\,dP$ is obtained by integration of the equation of state for pyrrhotite. For every datum on the FeS solubility in sphalerite, x_i, coexisting with pyrrhotite and Fe at temperature T_i and pressure P_i, the corresponding FeS solubility at 1 bar, $x_{0,i}$, can be evaluated from the linear equation 1 obtained by Balabin and Urusov (1995). On the basis of equation 19, the optimal set of model parameters should afford a minimum to the following function:

$$s_1 = \sum \left| \mu^{Sph}_{FeS}(P_i,T_i,x_i) - \mu^{Sph}_{FeS}(1\ \text{bar}, T_i, x_{0,i}) - \varphi(T_i,P_i) \right| \qquad (20)$$

Note that the standard Gibbs energy of the end-member (which is the hypothetical FeS with the sphalerite-type structure) cannot be evaluated by minimizing s_1, as it has been cancelled out on the left hand side of equation 19.

An object function similar to s_1 cannot be employed for the equilibrium sphalerite + pyrrhotite + pyrite because the corresponding 1 bar isobar of N^{Sph}_{FeS} in it has not been well

established. However, data on sulfur activity in S-rich pyrrhotite affords an accurate estimate for the pressure effect on the composition of pyrrhotite coexisting with pyrite, and of the chemical potential of FeS in pyrrhotite and in coexisting sphalerite.

Considering pyrite to be a stoichiometric FeS_2, the condition of equilibrium between it and non-stoichiometric pyrrhotite can be formulated as

$$\mu_{Fe}^{Po} + 2\mu_S^{Po} = G_{FeS_2} \qquad (21)$$

where G_{FeS_2} stands for the molar Gibbs energy of pyrite. Differentiating equation 21 with respect to P at constant T, and upon a rearrangement and use of the Gibbs-Duhem relation, the following expression may be obtained for concentration of Fe in pyrrhotite:

$$\left(\frac{\partial N_{Fe}^{Po}}{\partial P}\right)_{Po+Py} = \frac{1 - N_{Fe}^{Po}}{1 - 3N_{Fe}^{Po}} \times \frac{V_{FeS_2} - \bar{V}_{Fe}^{Po} - 2\bar{V}_S^{Po}}{\left(\frac{\partial \mu_{Fe}^{Po}}{\partial N_{Fe}^{Po}}\right)_{P;T}} \qquad (22)$$

where V_{FeS_2} is the molar volume of pyrite, V_{Fe}^{Po} is the partial molar volume of Fe in pyrrhotite, and $\bar{V}_S^{Po}$ is the partial molar volume of sulfur in pyrrhotite.

We have carried out a numerical integration of this relation in order to calculate the composition of pyrrhotite coexisting with pyrite at elevated pressures. The initial condition (i.e. the composition of pyrrhotite in this equilibrium at zero pressure) was taken from a least-squares fit to the data of Arnold (1962) and Toulmin and Barton (1964), the derivative

$$\left(\frac{\partial \mu_{Fe}^{Po}}{\partial N_{Fe}^{Po}}\right)_{P;T}$$

was estimated from the pyrrhotite model provided by Chuang *et al.* (1985), and we utilized the volumetric data discussed earlier. In Fig. 3 we show the calculated 2.5 kbar and 5 kbar isobars along with experimental findings by Scott (1973).

Close inspection of Fig. 4 reveals that 10 of the 14 available data points are situated in close proximity to their calculated isobars, while the remaining four are shifted to the Fe-rich side. Scott (1973), on the basis of his own thermodynamic calculations, suggested that most of the pyrrhotites in his experiments had re-equilibrated during the quench. However, compositions of pyrrhotite obtained by Udodov and Kashayev (1970) and Chernyshev *et al.* (1968) in their

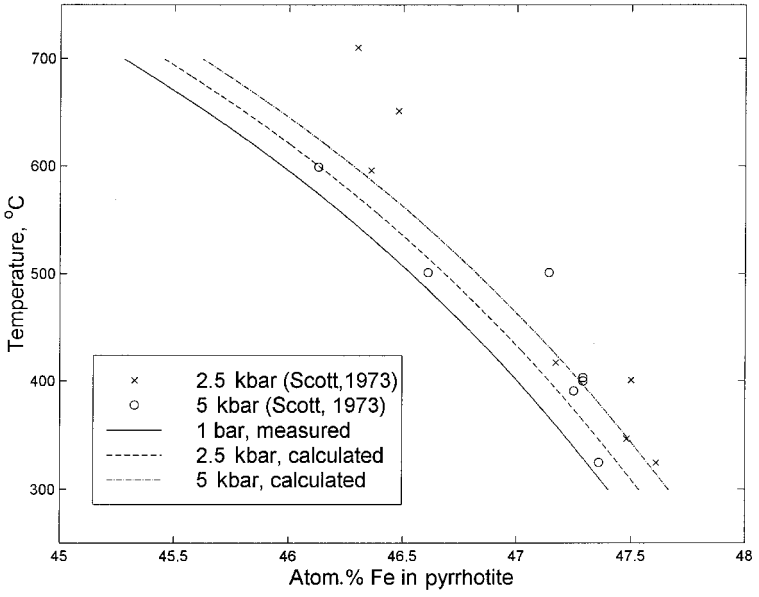

FIG. 3. Portion of the phase diagram of the system Fe-S showing the composition of pyrrhotite in equilibrium with pyrite as a function of temperature at pressures up to 5 kbar. The 1 bar isobar was obtained by a polynomial fit to the data of Arnold (1962) and Barton and Toulmin (1966). The isobars for higher pressures were calculated as described in the text, independently of the experimental data from Scott (1973) (circles and crosses).

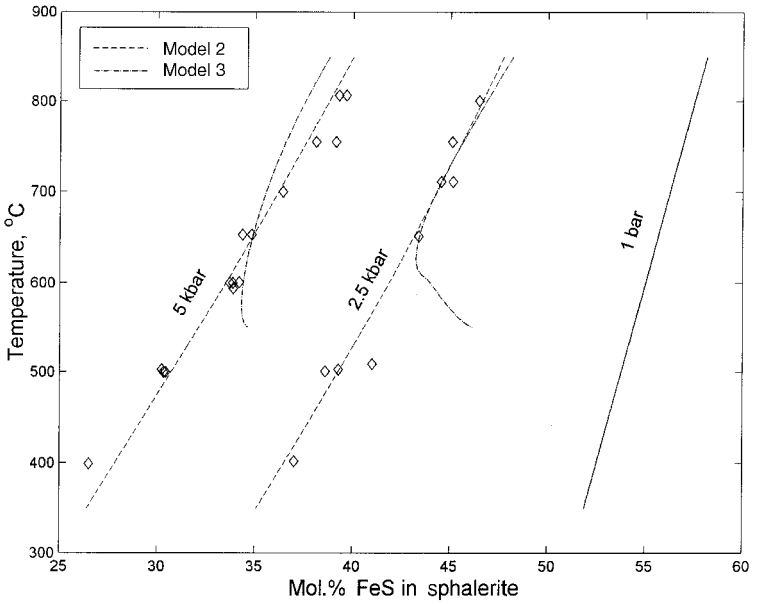

FIG. 4. A comparison between calculated FeS solubility in sphalerite coexisting with hexagonal pyrrhotite and Fe metal at 2.5 and 5 kbar and experimental data of Hutchison and Scott (1983). The compositions of sphalerite were calculated using Models 2 and 3 as described in the text taking the 1 bar isobar from Balabin and Urusov (1995) for the initial conditions. The isobars calculated using Model 3 are truncated at the maximal temperature of spinodal ordering.

experimental studies of the assemblage pyrrhotite + pyrite (1 kbar, hydrothermal) were found to be in excellent agreement with the results of Arnold (1962) and Toulmin and Barton (1964). In view of this, and our estimates, it seems more plausible that the above-mentioned 10 data points from Scott (1973) do represent equilibrium compositions, indirectly confirming the accuracy of our calculations. Even so, the uncertainty about the initial condition, which, as we noted above, may be up to 0.18 atom.% Fe, leads to a potential error in the estimate of μ_{FeS}^{Po} varying from 298 J/mol at 300°C to 506 J/mol at 700°C.

Insofar as the chemical potential of FeS in sphalerite is to be the same as that in coexisting pyrrhotite, the optimal set of model parameters should minimize the following function:

$$s_2 = \Sigma|\mu_{FeS}^{Sph}(P_j,T_j,x_j) - \mu_{FeS}^{Po+Py}(P_j,T_j)| \qquad (23)$$

where x_j is an experimentally determined concentration of FeS in sphalerite at given P_j,T_j and μ_{FeS}^{Po+Py} stands for the corresponding chemical potential of FeS in pyrrhotite whose composition has been calculated by numerical integration of equation 22. The values of chemical potential of FeS in sphalerite, $\mu_{FeS}^{Sph}(P_i,T_i,x_i)$, participating in the expressions for both s_1 and s_2 (equations 20 and 23) were corrected for thermal expansion and compressibility using data for pure ZnS with the sphalerite structure (Skinner, 1962; Bloc, 1989), assuming that these properties do not vary with FeS content.

Next, the cell edge of sphalerite with x mol.% FeS synthesized at temperature T can be calculated from its molar volume as

$$a_0(T,x) = 1.34054 \times V(1\ \text{bar},T,x)^{1/3}.$$

(Here the volume should not be corrected for thermal expansion because all the measurements of the unit-cell parameter of Fe-bearing sphalerite were taken on quenched samples at room conditions.) Therefore, the following function should be minimized in the appraisal of the sphalerite solution:

$$s_3 = \sum|a_{0,k} - 1.34054 \times V(1\ \text{atm},T_k,x_k)^{1/3}| \qquad (24)$$

We have carried out simultaneous minimization of the functions s_1, s_2 and s_3 given respectively by equations 20, 23 and 24 employing the Nelder-Mead simplex method implemented in the MATLAB system.

TABLE 5. Interaction parameters and interatomic distances of the (Zn,Fe)S sphalerite solution estimated using Model 2.

w_1^{tr} = 1.920.8 J/mol	d_{Zn-Zn} = 3.8250 Å
w_2^{tr} = 2,328.8 J/mol	d_{Zn-Fe} = 3.8445 Å
w_3^{tr} = 16,947 J/mol	d_{Fe-Fe} = 3.8329 Å

$\mu_{FeS,0}^{Sph} = -1.30922 \times 10^5 - 133.019T \ln T$

The database we utilized for parameter fitting includes 21 concentrations of FeS in sphalerite coexisting with pyrrhotite and metallic Fe at 2.5 and 5 kbar from Hutchison and Scott (1983), 47 concentrations of FeS in sphalerite equilibrated with pyrrhotite and pyrite reported by Scott and Barnes (1971), Boorman *et al.* (1971), Scott (1973), and Lusk and Ford (1978), and 47 cell edge measurements for Fe-bearing sphalerites synthesized at various temperatures under the sulfur pressure controlled by the Fe/FeS buffer from Barton and Toulmin (1966). Only compositions of sphalerite determined by microprobe were included in the database, in recognition of the less reliable nature of earlier data obtained by XRD and/or wet chemical analysis.

Results and discussion

Three different models of increasing intricacy were calibrated for the sphalerite solution in the present study. In each of these models the same treatments of entropy (equations 6–12) and volume (equation 18 and formulae in Table 3) were employed, but in the description of internal energy interactions were ascribed to the following 'species': (Model 1) ***nn*** + ***nnn***, (Model 2) ***tr*** + ***nnn***, and (Model 3) ***tr*** + ***csq***, as discussed in the section on the cuboctahedron + octahedron approximation. In addition to the energy parameters in these models (see below), two of the interatomic distances in the bond-length approximation for configurational volume (d_{Zn-Fe} and d_{Fe-Fe} in formulae from Table 3) were also regarded as adjustable parameters, while the third distance d_{Zn-Zn} = 3.825 Å was fixed by a_0 of pure ZnS (5.4093 Å, Barton and Toulmin, 1966).

The simplest of the models (Model 1) has four adjustable parameters (pairwise interaction parameters w^{nn} and w^{nnn}, equation 15, plus the distances d_{Zn-Fe} and d_{Fe-Fe}). It is inadequate. Not only does it fail to reproduce the experimental data on the equilibria sphalerite + pyrrhotite + metallic Fe and sphalerite + pyrrhotite + pyrite, but it does not even match the essential features of the latter equilibrium. In contrast, Model 2 with five fitting parameters (w^{nnn}, w_1^{tr} and w_2^{tr}, equation 16, and d_{Zn-Fe}, d_{Fe-Fe}) assembled in Table 5 reproduces the compositions of sphalerite in both of the equilibria within experimental accuracy (Figs 4 and 5), ±0.60 mol.% FeS for sphalerite equilibrated with pyrite + pyrrhotite and ±0.66 mol.% FeS for sphalerite equilibrated with pyrrhotite + Fe metal. Furthermore, the model correctly predicts that the cell edge in quenched Fe-sphalerites diminishes with increasing temperature of synthesis, but may not reproduce the amplitude of this variation (Fig. 6). μ_{FeS}^{Sph} (as it appears in equation 23) is reproduced by Model 2 to within ±80.7 J/mol for the equilibrium sphalerite + pyrrhotite + Fe metal and ±177.5 J/mol for sphalerite + pyrrhotite + pyrite. However, the actual precision of μ_{FeS}^{Sph} cannot be rigorously evaluated. The estimates of μ_{FeS}^{Sph} obtained rely largely on volumetric data of unknown accuracy. Also, in the case of the latter equilibrium, the possible error of 0.18 atom.% Fe in pyrrhotite coexisting with pyrite would produce, upon integration of equation 22, a systematic error in the calculated value of μ_{FeS}^{Po}, proportional to the pressure, with the mean value varying from 298 J/mol at 300°C to 506 J/mol at 700°C.

Model 2 predicts relatively small positive deviations from ideality in the sphalerite solution. The maximal value of excess Gibbs energy of mixing ranges from 1,506 J/mol at 900°C to 1,423 J/mol at 300°C (Fig. 7). The mean value of the Lewis and Randall activity coefficient for FeS varies from 1.32 at 900°C to 1.69 at 300°C, whereas the range of variation of the corresponding activity coefficient for ZnS is even smaller: 1.023 at 900°C to 1.034 at 300°C (Fig. 8). In fact, deviations from ideality for the ZnS component become negligible below ~40 mol.% FeS. These inferences are in surprisingly good agreement with preceding thermodynamic appraisals of Fe-sphalerite (Fleet, 1975; Balabin and Urusov, 1995). The fact that previous models failed to reproduce the FeS solubility in sphalerite coexisting with pyrrhotite and pyrite illustrates the importance of subtle changes in the activity with temperature and composition to thermodynamic analysis of phase equilibrium. The remarkably small temperature variation in the excess Gibbs energy (Fig. 7) implies a negative

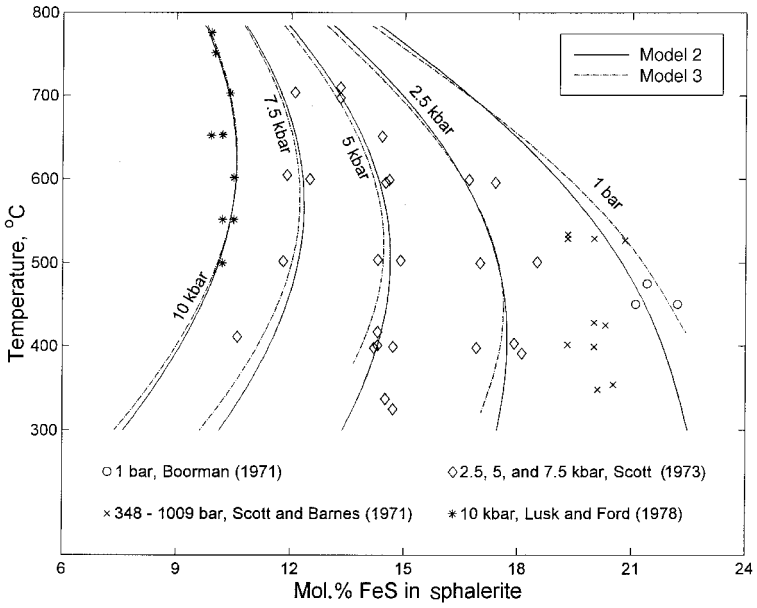

FIG. 5. A comparison of FeS solubility in sphalerite coexisting with hexagonal pyrrhotite and pyrite at pressures up to 10 kbar calculated using Models 2 and 3 with experimental data. The isobars obtained using Model 3 are truncated at the temperatures of spinodal ordering.

excess entropy of mixing in absolute value not exceeding 0.25–0.3 e.u. at all temperatures and compositions, in agreement with the finding that molar heat capacity of Fe-sphalerite is a near linear function of composition (Pankratz and King, 1965).

For practical use, the excess Gibbs energy of mixing of Fe-sphalerites corresponding to Model 2 has been approximated using a Guggenheim-type polynomial (Guggenheim, 1937)

$$G^{ex}_{(Zn,Fe)S} = x_{ZnS}x_{FeS}[A_0 + A_1(x_{ZnS} - x_{FeS}) + A_2(x_{ZnS} - x_{FeS})^2 + A_3(x_{ZnS} - x_{FeS})^3 + A_4(x_{ZnS} - x_{FeS})^4]$$

where x_{ZnS} and x_{FeS} are the mole fractions and the coefficients A_i are the following polynomials in T(K):

$$A_0 = 3464.954 + 4.9152T - 4.05220(T^2/10^3) + 1.20078(T^3/10^6)$$

$$A_1 = -4864.33 + 3.95230T - 3.50847(T^2/10^3) + 1.08473(T^3/10^6)$$

$$A_2 = 350.802 + 1.51804T - 1.57187(T^2/10^3) + 0.52146(T^3/10^6)$$

$$A_3 = 2326.79 - 5.65240T + 5.10041(T^2/10^3) - 1.59157(T^3/10^6)$$

$$A_4 = 3541.39 - 8.36153T + 7.44021(T^2/10^3) - 2.30296(T^3/10^6)$$

For the description of the mixing volume of (Zn,Fe)S sphalerites equation 12 in Hutchison and Scott (1983) is recommended.

Despite the apparent success of Model 2 in describing the experimental results for the assumption that Fe-sphalerite is a continuous homogeneous solution without any kind of long-range ordering, it predicts that such ordering will develop for some compositions at temperatures slightly below those of the experiments. This prediction is manifested by loss of thermodynamic stability of the disordered sphalerite solution.

When using CVM, sublattices must be introduced *a priori* in order to treat a given ordered structure. The disordered phase, prevailing at high temperatures, reaches its lowest temperature of possible existence, either stable or metastable, when its Gibbs surface G loses the property of being convex and the smallest eigenvalue of the second differential of G vanishes (cf. Sanchez and de Fontaine, 1980). The plot of this temperature *vs.* composition, the so-called "ordering spinodal" (de Fontaine, 1975), demarcates the

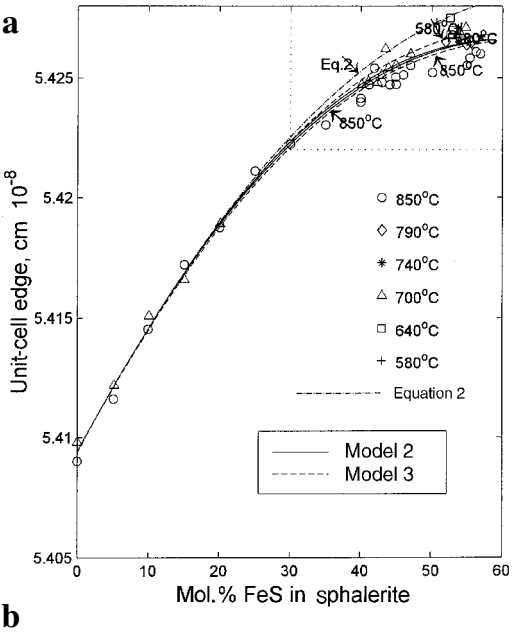

FIG. 6. (*a*) A comparison of lattice parameters for Fe-bearing sphalerites calculated with Models 2 and 3 for 580 and 850°C with experimental results of Barton and Toulmin (1966) for Fe-sphalerites synthesized under sulfur fugacities controlled by the Fe/FeS buffer (points) and those prepared at higher sulfur pressures (the dotted curve) and presumably re-ordered during the quench. (*b*) Enlarged portion of Fig. 6*a* in the rectangle defined by dotted lines.

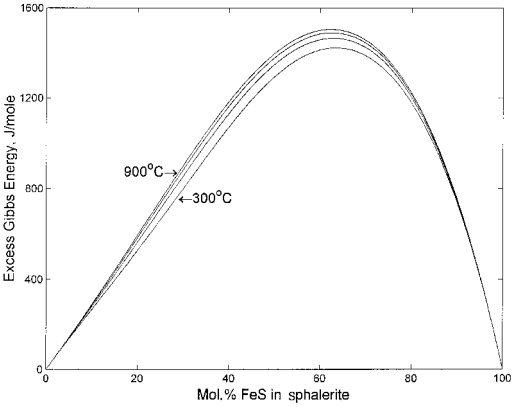

FIG. 7. The excess Gibbs energy of Fe-sphalerite as obtained using Model 2 at 300, 500, 700 and 900°C plotted against mol.% FeS in sphalerite.

boundary on the phase diagram below which only an ordered phase or an assemblage of the disordered and ordered phase(s) can be found.

Our attempts to keep the critical temperatures of ordering below 350–400°C while fitting the data with Model 3 (twelve adjacent parameters) or with a more sophisticated description of configurational volume have been unsuccessful. Moreover, any gain in accuracy of fitting that can be achieved with those models is accompanied by even higher critical temperatures than those obtained with Model 2. The profile of ordering spinodal is basically determined by the choice of data points not used in fitting. Shown in Fig. 9 are two typical profiles corresponding to best fits obtained with Model 3 for two different reduced data sets (the corresponding model parameters are given in the figure caption). The maxima discernible on these curves represent critical points where ordering occurs as a second- or higher-order transition. Such critical points mark the emergence of new phases. For instance, the sharp maximum at ~1.3 mol.% FeS points to stabilization of a superstructure with at least 70–75 atoms in a unit cell at 300–400°C. The best fit to the remaining data (i.e. those positioned above the critical spinodal) allows for slightly better descriptions of the equilibria sphalerite + pyrite + pyrrhotite (excluding 25–52% of data, Fig. 5), and sphalerite + pyrrhotite + Fe (excluding 33–62% of data, Fig. 4), but significantly improves the description of the temperature variation of cell-edge (excluding 4–6% of data), still allowing for no more than 20–35% of its experimentally observed magnitude (Fig. 6*a,b*).

Our conclusion is that the temperature variation of the cell edge and long-range ordering in Fe-sphalerites are real phenomena reflecting the non-additive nature of interactions in clusters as large

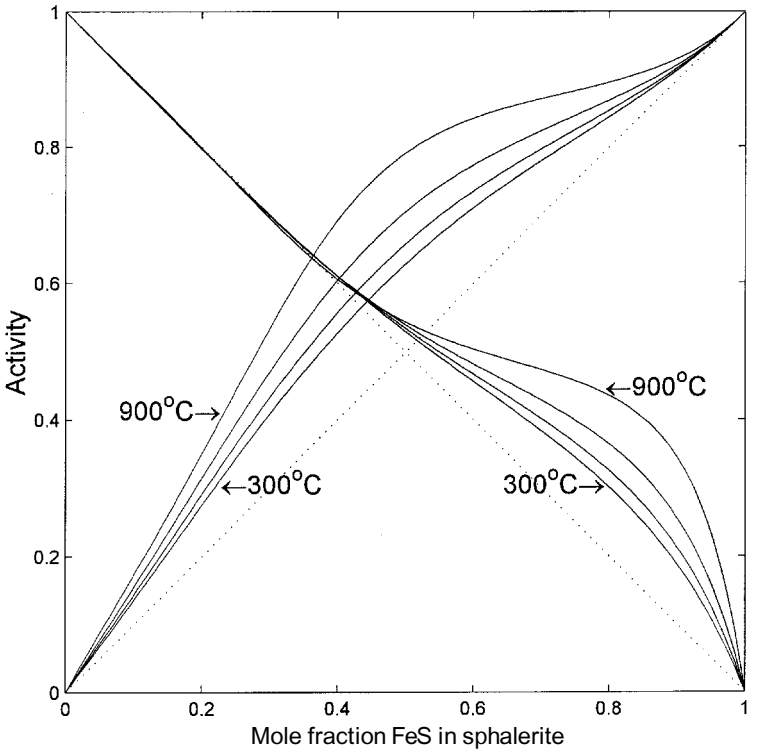

FIG. 8. Activities of FeS and ZnS in the (Zn,Fe)S sphalerite obtained using Model 2 at 300, 500, 700 and 900°C plotted against mole fraction of FeS in sphalerite.

as ***tr*** and ***csq***, containing three and five atoms, respectively. Little confidence can be placed in the calculated ordering spinodals as they are acutely sensitive to minor variations in energy parameters. It is also possible that we have underestimated the temperatures of spinodal ordering due to our treatment of some ordered phases as long-range disordered homogeneous sphalerites.

Indeed, it is noteworthy that Sorokin *et al.* (1975) have concluded that at least two crystallographically inequivalent positions are required to explain the presence of two doublets in the Mössbauer spectra of Fe-sphalerites they synthesized at 400–460°C using hydrothermal techniques. The presence of such ordered phases may well account for complexities and apparent discrepancies in results of experimental investigations of phase equilibria and cell dimensions of the (Zn,Fe)S solution. In the latter case, it is also possible that many of the disordered sphalerites synthesized at temperatures above the ordering spinodal have reordered during quench. Preservation of temperature variations of a_0 in Fe-sphalerites synthesized at the FeS/Fe buffer (Barton and Toulmin, 1966) presumably reflects blocking of the diffusion mechanisms in these sphalerites due to entry of neutral Fe atoms into interstitials.

The well known polytypism in sphalerite may in turn be related to the substitutions of Fe for Zn and the accompanying strong non-additive interactions in its cationic sublattice. It is noteworthy that the parameter w^{nnn}, the exchange energy of next to nearest neighbour atom pairs (equation 14) is estimated with Model 2 (Table 5) to be approximately eight times the values of parameters w_1^{tr} and w_2^{tr} accounting for the interactions among nearest neighbour atoms. This implies that ordering in sphalerite is driven primarily by a tendency to minimize the number of identical atoms in the second rather than the first coordination sphere in the cationic sublattice. While the first coordination spheres are similarly

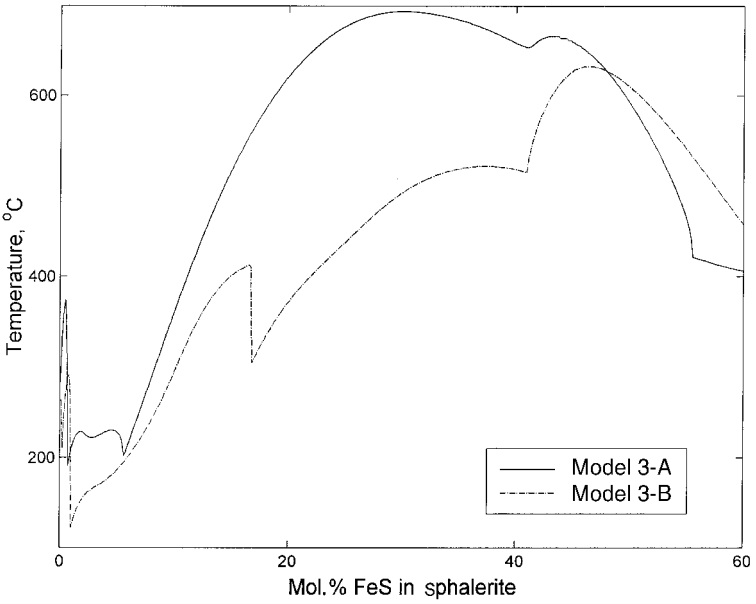

FIG. 9. Ordering spinodal demarcating possible long-range ordering in the sphalerite (Zn,Fe) solution obtained for Model 3 with the following two optimized sets of parameters:

Model 3-A:
$w_1^{tr+csq} = -1{,}217.3$ J/Mol.
$w_2^{tr+csq} = -1{,}029.3$ J/Mol.
$w_3^{tr+csq} = -6{,}817.0$ J/Mol.
$w_4^{tr+csq} = -1{,}733.9$ J/Mol.
$w_5^{tr+csq} = -1{,}902.5$ J/Mol.
$w_6^{tr+csq} = 26{,}780$ J/Mol.
$w_7^{tr+csq} = -18{,}903$ J/Mol.
$w_8^{tr+csq} = 1{,}044.4$ J/Mol.
$w_9^{tr+csq} = -13{,}540$ J/Mol.
$w_{10}^{tr+csq} = -1{,}098.0$ J/Mol.
$d_{Zn-Fe} = 3.8434$ eÅ and $d_{Fe-Fe} = 3.8332$ Å,
$\mu_{0,FeS}^{Sph} = -1.7369 \times 10^5 - 278.08T + 28.8807T \ln(T)$

Model 3-B:
$w_1^{tr+csq} = -1{,}648.5$ J/Mol.
$w_2^{tr+csq} = -35.097$ J/Mol.
$w_3^{tr+csq} = -6{,}045.6$ J/Mol.
$w_4^{tr+csq} = -2{,}401.6$ J/Mol.
$w_5^{tr+csq} = -3{,}746.6$ J/Mol.
$w_6^{tr+csq} = 17{,}449.6$ J/Mol.
$w_7^{tr+csq} = -18{,}981.6$ J/Mol.
$w_8^{tr+csq} = 1{,}694.7$ J/Mol.
$w_9^{tr+csq} = -11{,}503.1$ J/Mol.
$w_{10}^{tr+csq} = -1{,}000.7$ J/Mol.
$d_{Zn-Fe} = 3.844$ Å and $d_{Fe-Fe} = 3.833$ Å,
$\mu_{0,FeS}^{Sph} = -1.15472 \times 10^5 - 223.55T + 35.3667T \ln(T)$.

constructed in all the polytypes of ZnS including sphalerite itself, mutual arrangements of more distant atoms may vary significantly from one polytype to another, thereby providing the possibility of reducing the enthalpy of the solution without developing a long-range ordering within stacking layers — merely by changing the nature of interactions between ***nnn*** atoms. Clearly, such a mechanism might stabilize some of the polytypes at intermediate compositions, provided the exchange energy between ***nnn*** atoms in (Zn,Fe)S with würtzite structure is weaker than in sphalerite. The data on polytypism of natural würtzite and sphalerite seem to agree with this conjecture. When two or more polytypes are found together, they usually exhibit contrasting FeS contents (e.g. Chao and Gault, 1998; Hollenbaugh and Carlson, 1983). Moreover, the degree of hexagonality of sphalerites from different localities was found to correlate with Fe content, and the correlation patterns for epithermal sphalerites were different from those

discovered in higher temperature deposits (Platonov *et al.*, 1969).

The data available are insufficient to identify which type of structure variation does take place in (Zn,Fe)S sphalerites. Only diffraction experiments conducted on different compositions at varying temperatures can clarify whether the strong interactions associated with Zn,Fe substitutions conjure long-range ordering or polytypism in sphalerite below ~650°C. Both phenomena, however, will result in the appearance of new phases on the phase diagram. Rigorous thermodynamic modelling of such phases can be accomplished with the cluster variation method provided their structures have been identified. Until such information is available, Model 2 can be used as a first order approximation that quantitatively reproduces experimental data on phase equilibrium.

Our inference that many (Zn,Fe)S solutions may be ordered phases and not sphalerite may well explain the patterns of sharp compositional zoning in sphalerites from hydrothermal vein-type deposits, Mississippi Valley-type deposits, some Kuroko-type deposits, and sulfide deposits of the East Pacific Rise (black smokers). Experimentally-measured diffusion rates (Mizuta, 1988) appear to be inconsistent with the preservation of sharp compositional zoning in continuous sphalerites given likely temperatures of formation and cooling rates of these deposits. Particularly striking are the alternating layers of sphalerite recording pronounced, repetitive, stepwise changes in composition that have been used to correlate various horizons in fissure vein-type deposits (e.g. Barton *et al.*, 1977; Loucks, 1984). Also problematic is the apparent paucity of sphalerites with 4–7 mol.% FeS in such deposits (e.g. Borredon *et al.*, 1983; Loucks, 1984; O'Leary and Sack, 1987). These paradoxes may be eliminated by assuming that the contrasting zones in sphalerites are composed of different ordered phases which should be regarded as different minerals with distinct homogeneity ranges. Development of an ordered phase might also explain the pronounced lowering of the FeS content of sphalerite in its assemblage with pyrrhotite and pyrite between 250 and 300°C, inferred from low-temperature experiments and studies of geothermal systems (e.g. Scott and Kissin, 1973; Browne and Lovering, 1973). Polytypes will certainly hamper identification of such phases, either natural or synthetic, by masking their XRD patterns.

Acknowledgements

The authors are indebted to Dr Idjad Khakovich Sabitov and his associates for deriving expressions for the volume of the octahedron in its different configurations. We also acknowledge many fruitful discussions with Dr Victor Vinograd, the helpful suggestions of two anonymous reviewers and thorough copy editing of Kevin Murphy. This paper was supported by NSF grant EAR-96-27479 (ROS).

References

Anzai, S. and Ozawa, K , 1974. Effect of pressure on the Neel and ferrimagnetic Curie temperatures of $FeS_{1+\delta}$. *Phys. Stat. Sol.*, **24**, K31–4.

Arnold, R.G. (1962) Equilibrium relations between pyrrhotite and pyrite from 325° to 743°C. *Econ Geol.*, **57**, 72–90.

Balabin, A.I. and Urusov, V.S. (1995) Recalibration of the sphalerite cosmobarometer: Experimental and theoretical treatment. *Geochim. Cosmochim. Acta*, **59**, 1401–10.

Barker, J.A. (1953) Methods of approximation in the theory of regular mixtures. *Proc. R. Soc.*, **A216**, 45.

Barton, P.B., Jr. and Toulmin, P., III (1966) Phase relations involving sphalerite in the Fe-Zn-S system. *Econ. Geol.*, **61**, 815–49.

Barton, P.B., Jr., Bethke, P.M. and Roedder, E. (1977) Environment of ore deposition in the Creede mining district, San Juan Mountains, Colorado: Part III. Progress toward interpretation of the chemistry of the ore-forming fluid for the OH vein. *Econ. Geol.*, **72**, 1–24.

Bloc, S., Piermarini, G.J., Munro, R.G. and Fuller, E. (1989) Isothermal phase behavior of silver antimony sulfide (Ag_3SbS_3), zinc germanium phosphide ($ZnGeP_2$) and zinc sulfide. *Physica A*, **156**, 341–52.

Benbattouche, N., Saunders, G.A., Lambsom, E.F. and Hönle, W. (1989) The dependences of the elastic stiffness moduli and the Poisson ratio of natural iron pyrites FeS_2 upon pressure and temperature. *J. Phys. D: Appl. Phys.*, **22** 670–5.

Boorman, R.S. (1967) Subsolidus studies in the ZnS-FeS-FeS_2 system. *Econ Geol.*, **62**, 614–31.

Boorman, B.S., Sutherland, J.K. and Chernyshev, L.V. (1971) New data on the sphalerite-pyrrhotite-pyrite solvus. *Econ. Geol.*, **66**, 670–5.

Borredon, R., Laffite, M. and Moury, R. (1983) Composition des sphalerites du district mineral de Hualgayoc (Perou). *Min. Deposita*, **18**, 437–42.

Bronshtein, I.N. and Semendiyev, K.A. (1979) *Handbook of Mathematics*. Teubner, GDR (in Russian).

Browne, P.R.L. and Lovering, J.F. (1973) Composition of sphalerites from the Broadland geothermal field and their significance to sphalerite geothermometry and geobarometry. *Econ. Geol.*, **68**, 381–7.

Bryndzia, T.L., Scott, S.D and Spry, P.G. (1988) Sphalerite and hexagonal pyrrhotite geobarometer: Experimental calibration and application to the metamorphosed sulfide ores of Broken Hill, Australia. *Econ Geol.*, **83**, 1193–204.

Burgman, E., Jr., Urbain, G. and Fronberg, M.G. (1968) Contribution à l'étude du systéme fer-soufre limité au domaine du mono-sulfure de fer (pyrrhotine). *Mem. Sci. Rev. Métall.*, **65**, 567–78.

Chao, G.Y. and Gault, R.A. (1998) The occurrence of two rare polytypes of wurtzite, 4H and 8H, at Mont Saint-Hilaire, Quebec. *Canad. Mineral.*, **36,** 775–8.

Chernychev, L.V., Anfilogov, V.A., Pastushkova, T.M. and Suturina, T.A. (1968) Hydrothermal investigation of the system Fe-Zn-S. *Geologiya Rudnykh Mestorozhdeniy*, **3**, 50–64 (in Russian).

Chernychev, L.V., Afonina, G.G. and Berestennikov, M.I. (1969) Cell-edge dimensions of iron-bearing sphalerites synthesized under hydrothermal conditions. *Geologiya Rudnykh Mestorozhdeniy*, **6**, 85–9 (in Russian).

Chuang, Y.Y., Hsieh, D.-C. and Chang, Y.A. (1985) Thermodynamic and phase relationships of transition metal sulfur systems: Part V. A re-evaluation of the Fe-S system using an associated solution model for the liquid phase. *Metall. Trans. B*, **1613**, 277–85.

Cromwell, P.R. (1997) *Polyhedra*. Cambridge University Press, Cambridge, UK.

Dicarlo, J., Albert, M., Dwight, K. and Wold, A. (1990) Preparation and properties of iron-doped II-VI chalcogenides. *J. Solid State Chem.*, **87**, 443–8.

Finel, A. (1994) The cluster variation method and some applications. Pp. 495–450 in: *Statics and Dynamics of Alloy Phase Transformations* (P.E.A. Turchi and A. Gonis, editors). Plenum Press, New York.

Finel, A. and Tetot, R. (1996) The Gaussian cluster variation method and its application to the thermodynamics of transition metals. Pp. 197–203 in: *Stability of Materials* (Ginis, editor). Plenum Press, New York.

Fleet, M.E. (1968) On the lattice parameters and superstructures of pyrrhotites. *Amer. Mineral.*, **53**, 1846–55.

Fleet, M.E. (1975) Thermodynamic properties of (Zn,Fe)S solid solutions at 850°C. *Amer. Mineral.*, **60** 466–70.

De Fontaine, D. (1975) *k*-Space symmetry rules for order-disorder reactions. *Acta Metall.*, **23**, 553–71.

De Fontaine, D. (1994) Cluster approach to order-disorder transformations in alloys. *Solid State Phys.*, **47**, 33–176.

Guggenheim, E.A. (1937) Theoretical basis of Raoult's law. *Trans. Faradary. Soc.*, **33**, 151–79.

Hijmans, J. and de Boir, J. (1955) An approximation method for order-disorder problems I. *Physica*, **21**, 471–84.

Hollenbaugh, D.W. and Carlson, E.H. (1983) The occurrence of wurtzite polytypes in eastern Ohio. *Canad. Mineral.*, **21**, 697–703.

Hutchison, M.N. and Scott, S.D. (1983) Experimental calibration of the sphalerite cosmobarometer. *Geochim. Cosmochim. Acta*, **47**, 101–8.

Keller-Besrest, F. and Collin, G. (1990) Structural aspects of the α-transition in stoichiometric FeS: Identification of the high-temperature phase. *J. Solid State Chem.*, **84**, 194–210.

Kikuchi, R.D. (1951) A theory of cooperative phenomena. *Phys. Rev.*, **81**, 988–1003.

Kikuchi, R. (1973) Superposition approximation and natural iteration calculation in cluster-variation method. *J. Chem. Phys.*, **60** 1071–80.

King, H.E., Jr and Prewitt, C.T. (1982) High-pressure and high-temperature polymorphism of iron sulfide (FeS). *Acta Crystallogr.*, **B38**, 1877–86.

Kruse, O. (1990) Mössbauer and X-ray study of the effects of vacancy concentration in synthetic hexagonal pyrrhotites. *Amer. Mineral.*, **75**, 755–63.

Libowitz, G.G. (1972) Energetics of defect formation and interaction in nonstoichiometric pyrrhotite. Pp. 107–15 in: *Reactivity of Solids* (J.B. Anderson, M.W. Roberts and F.S. Stone, editors). Chapman & Hall, London.

Loucks, R.R. (1984) *Zoning and ore genesis at Topia, Durango, Mexico*. PhD Thesis, Harvard Univ., Cambridge, Massachusetts.

Lusk, J. and Ford, C.E. (1978) Experimental extension of the sphalerite geobarometer to 10 kbar. *Amer. Mineral.*, **63**, 516–9.

Massalski, T.B. ed. (1986) *Binary Alloy Phase Diagrams*. American Society for Metals, Metals Park, Ohio.

Mizuta, T. (1988) Interdiffusion rate of zinc and iron in natural sphalerite. *Econ. Geol.*, **83**, 1205–20.

Niwa, K. and Wada, T. (1961) Thermodynamic studies of pyrrhotite. *Metall. Soc. Conf.*, **8**, 945–61.

Novikov, G.V., Sokolov Ju.A. and Sipavina, L.V. (1982) The temperature dependence of the unit-cell parameters of pyrrhotite $Fe_{1-x}S$. *Geochem. Int.*, **19**, 184–90.

Novikov, G.V., Egorov, V.K. and Sokolov, Ju.A. (1988) *Pyrrhotites: Crystal and Magnetic Structure. Phase Transformations*. Nauka, Moscow (in Russian).

Oates, W.A., Zhang, F., Chen, S.-L. and Chang, Y.A. (1999) Improved cluster-site approximation for the entropy of mixing in multicomponent solid solutions. *Phys. Rev. B*, **59**, 11221–25.

O'Leary, M.J. and Sack, R.O. (1987) Fe-Zn exchange reaction between tetrahedrite and sphalerite in natural

environments. *Contrib. Mineral. Petrol.*, **96**, 415–25.
Osadchii, E.G. and Sorokin, V.I. (1989) *Stannite-Containing Sulfide Systems*. Nauka, Moscow (in Russian).
Pankratz, L.B. and King, E.G. (1965) High-temperature heat contents and entropies of two zinc sulfides and four solid solutions of zinc and iron sulfides. *Bureau of Mines Report of Investigations*, **6708**, 1–8.
Platonov, A.N., Shadlun, T.N., Polyakova, O.P., Dobrovol'skaya, M.G. (1969) Polytypes of sphalerites and their typomorphic importance. *Geologiya Rudnykh Mestorozhdeniy*, **11**, 3–16 (in Russian).
Rau, H. (1976) Energetics of defect formation and interaction in pyrrhotite $F_{1-x}S$ and its homogeneity range. *J. Phys. Chem. Solids*, **37**, 425–9.
Rosenqvist, T. (1954) A thermodynamic study of iron, cobalt and nickel sulfides. *J. Iron Steel Inst.*, **176**, 37–57.
Saati, Th.L. and Bram, J. (1964) *Nonlinear Mathematics*. Dover Publications, New York.
Sanchez, J.M., Ducastelle, F. and Gratias, D. (1984) *Physica A*, **128**, 334.
Sanchez, J.M. and de Fontaine, D. (1980) Ordering in fcc lattices with first- and secopnd-neighbor interactions. *Phys. Rev. B*, **21**, 216–28.
Schlijper, A.G. and Westerhof, J. (1987)Improved cluster variation approximations by extention of local thermodynamic states. *Phys. Rev. B*, **36**, 5458–65.
Schneeberg, E.P. (1973) Sulfur fugacity measurements with the electrochemical cell Ag|AgI|$Ag_{2+x}S$. *Econ. Geol.*, **68**, 507–17.
Scott, S.D. and Barnes, H.L. (1971) Sphalerite geothermometry and geobarometry. *Econ. Geol.*, **66**, 653–69.
Scott, S.D. (1973) Experimental calibration of the sphalerite geobarometer. *Econ. Geol.*, **68**, 466–74.
Scott, S.D. and Kissin, S.A. (1973) Sphalerite composition in the Zn-Fe-S system below 300°C. *Econ. Geol.*, **68**, 475–9.
Skinner, B.J. (1962) Thermal expansion of ten minerals. *USGS Prof. Paper*, **450-D**, 109–12.
Sorokin, V.I. and Bezmen, N.I. (1973) The sulfide system Zn-Fe-S in equilibrium with chloride solutions at 600°C and 1000 kg/cm^2. *Ocherki Fiziko-ximicheskoy Petrologii*, **3**, pp. 36–43. Nauka, Moscow (in Russian).
Sorokin, V.I. and Chichagov, A.V. (1974) Sulfides from the system Zn-Fe-S in equilibrium with water solution of NH_4Cl at 400°C and 1000 kg/cm^3. *Ocherki fiziko-ximicheskoj petrologii*, **4**, 176–85. Nauka, Moscow (in Russian).
Sorokin, V.I., Gruzdev, V.S. and Shorygin, V.A. (1970) Variation of the a_o parameter with the content of iron in sphalerite obtained under hydrothermal conditions. *Geochem. Int.*, **7**, 361–3.
Sorokin, B.I., Novikov, V.K., Egorov, V.K., Popov, V.I. and Sipavina, L.V. (1975) An investigation of Fe-sphalerites by means of Mössbauer spectroscopy. *Geochimiya*, **9**, 1329–35.
Taylor, L.A. (1969) Low-temperature phase relations in the Fe-S system. *Carnegie Inst. Wash. Yearb.*, **62**, 175–89.
Toulmin, P., III and Barton, P.B., Jr. (1964) A thermodynamic study of pyrite and pyrrhotite. *Geochim. Cosmochim. Acta*, **28**, 641–71.
Toulmin, P., III, Barton, P.B., Jr. and Wiggins, L.B. (1991) Commentary on the sphalerite geobarometer. *Amer. Miner.*, **76**, 1038–51.
Turkdogan, E.T. (1968) Iron-sulfur system. Part 1: Growth of ferrous sulfide in iron and diffisivities of iron in ferrous sulfide. *Trans. Metall. Soc. Amer. Ins. Min. Metall. Pet. Eng.*, **242**, 1665–72.
Udodov, Yu.,N. and Kashayev, A.A. (1970) An isothermal section (400°) of the state diagram of pyrrhotite. *Trans. (Doklady) U.S.S.R. Acad. Sci.: Earth Sci. Sect.*, **187**, 103–5.
Vaks, V.G. and Samolyuk, G.D. (1999) On accuracy of different cluster models used in describing ordering phase transitions in fcc alloys. *JETP*, **88**, 89–100.
van Aswegen, J.T.S. and Verleger, H. (1960) Röntgenographishe untersuchung des systems ZnS-FeS. *Die Naturwissenschaften*, **47**, 131.
Vinograd, V.L. and Putnis, A. (1999) The description of Al, Si ordering in aluminosilicates using the cluster variation method. *Amer. Mineral.*, **84**, 311–24.
Zunger, A. (1994) First-principles statistical mechanics of semiconductor alloys and intermetallic compounds. Pp. 361–419 in: *Statics and Dynamics of Alloy Phase Transformations* (P.E.A. Turchi and A. Gonis, editors) Plenum Press, New York.

[*Manuscript received 20 October 1999: revised 23 March 2000*]